J. Phys. B: At. Mol. Opt. Phys. **40** (2007) 3283–3293 doi:10.1088/0953-4075/40/16/009

Experimental evidence for an isotopic effect in the formation of ultracold ground-state rubidium dimers

A Fioretti[1], **O Dulieu**[2,3] **and C Gabbanini**[1]

[1] Istituto per i processi chimico-fisici del CNR, Via Moruzzi 1, 56127 Pisa, Italy
[2] Laboratoire Aimé Cotton, CNRS, Bât. 505, Campus d'Orsay, F-91405 Orsay Cedex, France

Received 9 May 2007, in final form 5 July 2007
Published 6 August 2007
Online at stacks.iop.org/JPhysB/40/3283

Abstract

We perform a comparative study of the formation of ultracold rubidium dimers in their ground state with both ^{85}Rb and ^{87}Rb isotopes. Ultracold rubidium molecules are created through photoassociation of ultracold atoms into rovibrational levels of the $0_u^+(5S_{1/2} + 5P_{1/2})$ excited state, which interact through resonant coupling (Dion *et al* 2001 *Phys. Rev. Lett.* **86** 2253) with rovibrational levels of the $0_u^+(5S_{1/2} + 5P_{3/2})$ excited state. The photoassociated levels decay by spontaneous emission down to rovibrational levels of the $X^1\Sigma_g^+$ ground state. The resonant coupling is expected to enhance the formation of ultracold molecules in low-lying ground-state levels. By modelling the ionization spectrum of these ultracold molecules, we show that this coupling is larger for $^{87}Rb_2$ molecules than for $^{85}Rb_2$ molecules.

(Some figures in this article are in colour only in the electronic version)

1. Introduction

In the last decade, various techniques to produce cold and ultracold molecules (i.e. with translational kinetic energy E_t equivalent to temperature of the order of, or much lower than $T = E_t/k_B \simeq 1$ mK, where k_B is the Boltzmann constant) have been implemented [1]. The creation of cold molecular samples offers new prospects for precision measurements, which benefit from the possibility to observe them for long durations. For instance, a non-zero value for the electric dipole moment of the electron could be discovered using cold beams or trapped ensembles of heavy polar molecules [2, 3], as a test of the validity of the standard model. Besides these metrology experiments, laser-cooled atoms also lead to a new approach for high-resolution molecular spectroscopy, the so-called photoassociation spectroscopy [4]. Ultracold polar molecules also represent a system of choice for the study of long-range interactions in dilute systems such as dipole–dipole interaction which could provide the basis for the elaboration of novel qubit realizations [5].

[3] Laboratoire Aimé Cotton is associated to Université Paris-Sud.

In order to create cold molecular samples, some methods slow down the molecules making use of their interaction with external fields, like the Stark deceleration technique for polar molecules [6]. Another approach starts from laser-cooled atoms and converts them into dimers through either magnetoassociation or photoassociation and radiative decay. The first recipe makes use of magnetic Feshbach resonances to match the energy of an open collisional channel to the energy of a bound molecular state; the molecules are so formed in the highest vibrational level. By this method also molecular condensates have been produced, starting from a quantum degenerate Fermi gas [7, 8]. In the photoassociation (PA) process, colliding pairs of cold free atoms are bound into excited dimers that can spontaneously decay into ground-state molecules [9]. The produced molecules are translationally cold, while their population spreads over some high vibrational states of the ground singlet or triplet states. The created dimers are also rotationally cold, as the colliding atomic pairs have unsufficient kinetic energy to get over the centrifugal barrier of high angular momentum states.

The formation of cold molecules using PA has been observed for all homonuclear alkali dimers [10], and recently also in some heteronuclear cases: KRb [11, 12], RbCs [13], NaCs [14] and LiCs [15]. Although a small fraction of the colliding atoms can be converted into dimers in almost all conditions, the efficiency of the process can be greatly enhanced in some particular cases provided the PA pumping rate is sufficiently high. A representative example is yielded by PA into the $0_g^-(nS + nP_{3/2})$ state of the heaviest alkali dimers Cs_2 and Rb_2 (with $n = 6$ and 5, respectively) [16–18]. This state has a double well potential curve which induces a large amplitude of the relevant radial wavefunction in a range of intermediate interatomic distances where the probability to decay into ground triplet state molecules is favourable. Another example is the mechanism of resonant coupling [19]: the coupling between long-range vibrational levels of the 0_u^+ state correlated to the $Cs(6S_{1/2} + 6P_{1/2})$ asymptote (hereafter referred to as the $P_{1/2}$ asymptote) to shorter-range vibrational levels of the accompanying 0_u^+ state dissociating into $Cs(6S_{1/2} + 6P_{3/2})$ (hereafter referred to as the $P_{3/2}$ asymptote), favours the efficient formation of singlet ground-state molecules well below the dissociation limit.

The PA spectroscopy of the coupled 0_u^+ rubidium dimer excited states recorded by the trap-loss technique has been recently interpreted in [20] for ^{85}Rb, and in [22] for ^{87}Rb. The formation of ultracold $^{85}Rb_2$ singlet ground-state molecules has been demonstrated in [21] through their detection by photoionization. On the theoretical side, pump–dump PA with short pulses on the coupled 0_u^+ states of ^{85}Rb has been proposed as a possible dimer formation mechanism in [23] and as a tool to optimize the stabilization step towards deep levels of the ground state [24].

In the present paper, we performed a comparative study of the formation of ultracold ground-state molecules with both ^{85}Rb and ^{87}Rb isotopes, through resonant coupling of the relevant 0_u^+ states. As described in section 2, we recorded the molecular ion signal yielded by the PA of the 0_u^+ state near the $P_{1/2}$ asymptote, followed by spontaneous emission to ground-state rovibrational levels which are then ionized after a resonantly-enhanced two-photon ionization. Using a coupled-state model, we emphasize the strength of the resonant coupling, which is found to be different for the two rubidium isotopes (section 3).

2. Experimental apparatus and results

The experiment is done in a UHV metal chamber, where a rubidium vapour pressure is established by running current through metal dispensers. The combination of three orthogonal pairs of laser beams for trapping, with suitable polarizations, and a repumping laser, in the presence of a magnetic field gradient produces a magneto-optical trap of ^{85}Rb or ^{87}Rb, according to the frequency tuning of the lasers. The trap holds nearly 10^7 atoms with a

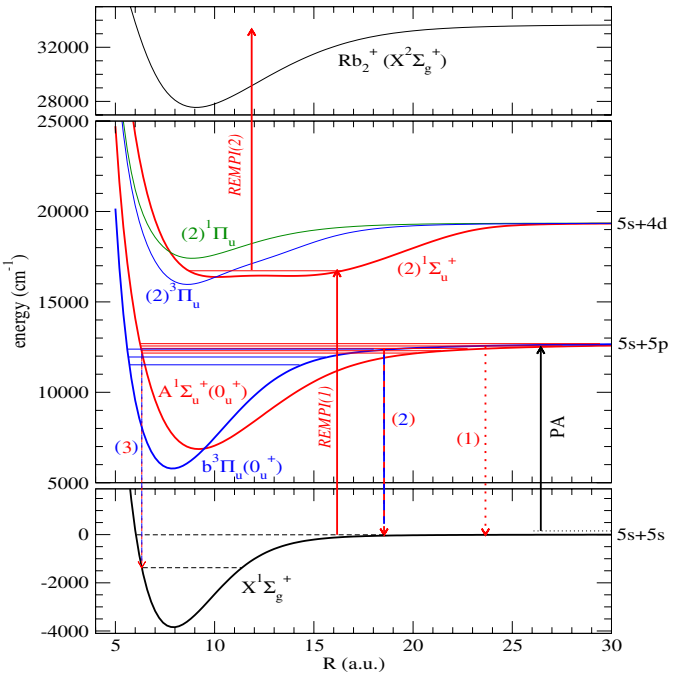

Figure 1. Rb_2 molecular potential curves (from [28]) involved in the cold molecule formation process and in their detection. All potentials are drawn at the same scale. Levels in the excited states are not drawn to scale; they illustrate the different level density in the $A^1\Sigma_u^+(0_u^+)$ and $b^3\Pi_u(0_u^+)$ states. Arrows correspond to spontaneous emission starting respectively from the external turning point of the PA level down to the uppermost vibrational level of the X state (1), from the intermediate turning point of the PA level induced by the resonant coupling down to moderately bound vibrational levels of the X state (2), and from the inner turning point of the PA level induced by the resonant coupling down to strongly bound vibrational levels of the X state (3). The latter cannot be ionized with the present REMPI laser. The other *ungerade* electronic states correlated to the 5s + 4d limit are also displayed for completeness.

density of 3×10^{10} cm^{-3} and a temperature of about 100 μK. A PA laser, constituted by a semiconductor laser of 50 mW maximum power (Mitsubishi 64114R), is directed into the trapped sample. The PA laser has a wavelength of about 795 nm which can be tuned by changing its temperature and which is measured by a wavemeter. A beam splitter sends part of the laser to a heated iodine cell to check the absolute frequency with the well-known I_2 absorption spectrum [25], and to a Fabry–Perot interferometer to check the scan linearity. Unfortunately, the limited tuning range of the diode laser allowed to scan just a portion of the frequency region of interest. Molecules produced in the ground state are detected by converting them into molecular ions by a resonantly enhanced multiphoton ionization (REMPI) process; the ions are time-of-flight selected and detected by a channeltron multiplier. The REMPI process is produced by a pulsed dye laser pumped by the second harmonics of a Nd:YAG laser running at 20 Hz repetition rate with 5 ns pulses. The dye laser, operating with Rhodamine 610 dye and having a pulse energy of about 2 mJ and a linewidth of 0.3 cm^{-1}, is softly focused on the MOT. Its wavelength is settled at about 598 nm, in order to resonantly excite the $X^1\Sigma_g^+$ ground-state molecules towards the $2^1\Sigma_u^+$ state [21, 26], from which a second photon of the dye laser completes the REMPI process. The relevant potential curves are displayed in figure 1, as well as a scheme of the steps of the present process.

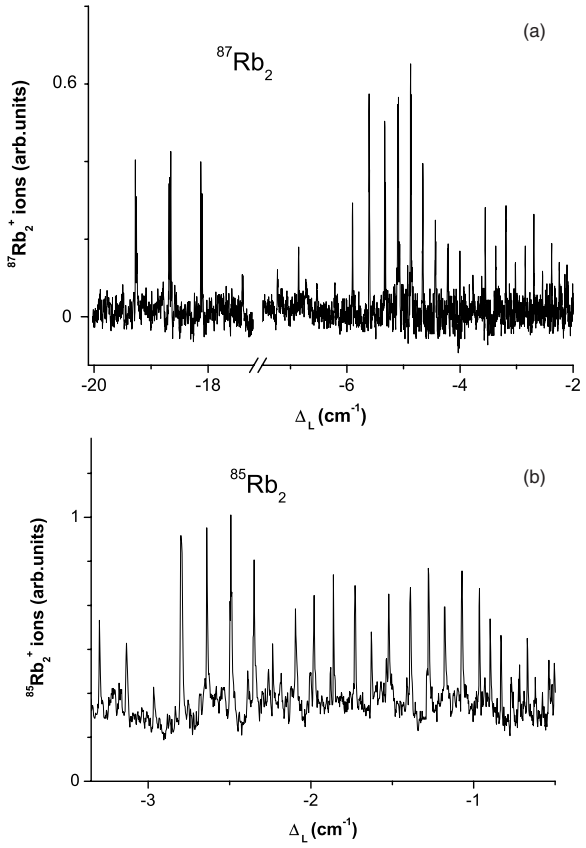

Figure 2. Molecular ions detected as a function of the PA laser detuning below the D_1 atomic line frequency for ^{87}Rb (a) and ^{85}Rb (b) isotopes. The origin of energy corresponds respectively to the $5S_{1/2}$ $(F = 2) \rightarrow 5P_{1/2}$ $(F = 2)$ transition at 12 578.88 cm^{-1} for ^{87}Rb and $5S_{1/2}$ $(F = 3) \rightarrow 5P_{1/2}$ $(F = 3)$ transition at 12 578.91 cm^{-1} for ^{85}Rb [27].

In spite of the low power of the available PA laser, cold molecules are observed with a good signal-to-noise ratio. The experimental spectra recorded by scanning the PA laser frequency on the red side of the atomic D_1 line are shown in figure 2 for both rubidium isotopes.

The spectra of the two isotopes look different beyond the fact that they are shown in dissimilar ranges. For ^{87}Rb there is a narrow frequency interval near a detuning of -4.8 cm^{-1} where there is an evident enhancement of the molecular ion signal. Another region of enhancement occurs near a detuning of -18.6 cm^{-1}. The $^{85}Rb_2$ cold molecules are produced quite efficiently for a larger frequency range and the maximum formation rate occurs at a detuning of about -2.5 cm^{-1}. The baseline of the spectrum differs from zero because some $^{85}Rb_2$ dimers are observed also in the absence of the PA laser. A more detailed discussion about the spectra will be presented in the next section.

A spectrum of $^{87}Rb_2$, recorded by keeping the PA laser frequency fixed at a detuning of -4.87 cm^{-1}, and scanning the pulsed dye laser frequency, is shown in figure 3. The spectrum is due to the $2^1\Sigma_u^+ \leftarrow X^1\Sigma_g^+$ band absorption. Following the analysis done in [21], the main peaks correspond to different vibrational levels of the excited $2^1\Sigma_u^+(5s + 4d)$ state. The width

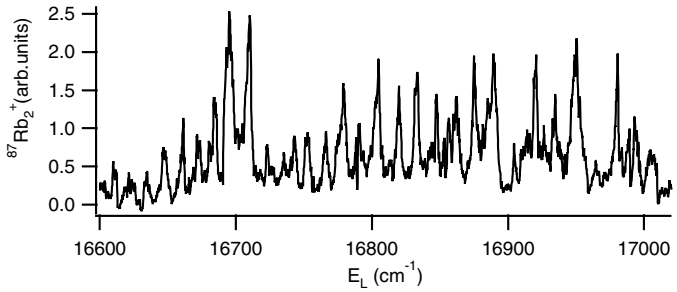

Figure 3. Molecular $^{87}Rb_2^+$ ions detected as a function of the dye laser frequency for a PA laser detuning of -4.87 cm^{-1}.

of the lines reflects the vibrational population of the ground-state molecules, which is here unresolved due to the pulsed laser linewidth.

3. Modelling and comparison with the experiment

The 0_u^+ Hund's case c states in alkali atom dimers result from the spin–orbit coupling between the Hund's case a $A^1\Sigma_u^+$ and $b^3\Pi_u$ states. The magnitude of the coupling is comparable to the typical spacing of the vibrational levels of these states over a large range of binding energies, so that the energy spectrum of the coupled states is very irregular, in contrast with lighter alkali dimers (see for instance [29]). Such perturbations have been observed by the Fourier transform spectroscopy in -2500 cm^{-1} to -1500 cm^{-1} binding energy range below the $P_{1/2}$ asymptote [30]. When approaching binding energies close to the $P_{1/2}$ asymptote, the level density of the $0_u^+(P_{1/2})$ state is much larger than the level density of the $0_u^+(P_{3/2})$ state, so that a perturbation is detected each time the PA laser hits a binding energy range in coincidence with $P_{3/2}$ short-range levels. Strong modulations of the rotational constant $B_v = \langle v|1/(2\mu R^2)|v\rangle$ of vibrational levels v below the $P_{1/2}$ are also a manifestation of this coupling, observed in the PA experiment of [20, 31]. Yet another signature is the predissociation of vibrational levels below the $P_{3/2}$ asymptote into the dissociation continuum of the $P_{1/2}$ asymptote [22]. On the theoretical side, most of these effects were predicted for cesium and rubidium dimers, including also a strong isotopic dependence, in the bound-state spectrum [32] as well as in the continuum [33, 34].

We model the formation of Rb_2 singlet ground-state molecules by including the PA step from the $X^1\Sigma_g^+$ dissociation continuum towards levels of the 0_u^+ coupled states at a fixed detuning δ_L below the $P_{1/2}$ asymptote, followed by spontaneous emission back to $X^1\Sigma_g^+$ bound levels. The vibrational distribution of the cold molecules in the $X^1\Sigma_g^+$ state is then determined by the decay probability of the initial photoassociated level. We neglect here the role of the rotation of the molecule, as well as its hyperfine structure. None of these features can be resolved by the ionization laser, and we expect that the relative intensity of the measured lines will not be influenced by them. Furthermore, the ionization probability is assumed uniform for all populated X vibrational levels, as in the previous works on Cs_2 for instance [19]. The cold molecule formation rate is then controlled by the product of the Franck–Condon factors for the PA step and decay step.

The energy and wavefunctions of the levels of the 0_u^+ coupled states and X state are computed using the Mapped Fourier Grid Hamiltonian (MFGH) method already described

elsewhere [35]. The MFGH approach is well suited for the description of levels close to the dissociation limit, due to its variable grid step adapted to the local kinetic energy of the radial motion, as well as to coupled-state calculations due to its matrix formulation. The evaluation of Franck–Condon factors is straightforward, as it reduces to the sum of products of relevant wavefunctions at the grid points. As in [36], we extend the calculation into the continuum of the X state, in order to represent the initial wavefunction on the same grid than the bound levels. We defined a grid extending from $5a_0$ to $2500a_0$ ($a_0 = 0.052\,9177$ nm) with 1431 points, allowing a reliable description of the continuum wavefunctions up to about 0.1 cm^{-1} above the ground-state asymptote. The resulting density of states in the continuum energy domain was high enough to select an initial wavefunction with an energy relevant for our experiment, i.e. the s-wave scattering state with a collision energy $E_{coll} = k_B T$ associated to the experimental temperature value (100 μK).

In our model, the potential energy surface (PES) of the $X^1\Sigma_g^+$ state is the one from the Fourier transform spectroscopy derived in [37], smoothly matched to the long-range form $-C_n/R^n$ (with $n = 6, 8, 10$) with C_n coefficients of [38]. The repulsive wall of this potential has been slightly shifted in R in order to reproduce the singlet scattering length for both isotopes [38]. The PES for the $A^1\Sigma_u^+$ and $b^3\Pi_u$ states of Edvardsson *et al* [39] are given as supplementary tables in [20] after a deperturbation analysis of PA results. The radial variation of the diagonal and off-diagonal spin–orbit couplings are also those employed in [20], resulting of the scaling of the computed couplings for K_2 [40] to the atomic rubidium fine structure splitting $\Delta E_{SO} = 237.598$ cm^{-1}. Such a choice is actually more efficient to reproduce the low-resolution absorption spectrum in Rb_2 [41] than the scaling from the computed Cs_2 spin–orbit couplings as in [35]. The radial variation of the transition dipole moment has been taken into account, although it could be safely neglected at least for the PA step which generally takes place at large distances.

It is well known from the standard spectroscopic studies (see for instance [30]) that the spin–orbit interaction induces a resonant coupling between levels of the coupled electronic states, which gives rise to perturbations in their energy spectra. The associated radial wavefunctions are strongly affected which results in oscillating patterns in the observed rotational constants [35]. An example of such a behaviour is yielded by the recent analysis of the PA spectrum of $^{85}Rb_2$ in [20]. The vibrational distribution of the produced cold molecules strongly depends on this coupling, as illustrated in figure 4(b): we display the decay probability, i.e. the bound–bound Franck–Condon factors (including transition dipole moment) between the $X^1\Sigma_g^+$ vibrational levels and a strongly resonant level of the coupled system (labelled by $n = 411$ in our model) excited by PA at a detuning of -54.26 cm^{-1} (resonance $n = 15$ at an energy 12 524.807 cm^{-1} in [20]). As the coupling modifies the vibrational wavefunction of the PA excited state by producing a peak in the amplitude at about $20a_0$, the stabilization by spontaneous emission occurs towards levels with binding energy up to about 15 cm^{-1} (red trace with full squares). The neighbouring level $n = 414$, at a detuning of -49.00 cm^{-1} (not reported in [20]) is much less resonantly coupled, so that the decay down to the same range of ground-state vibrational levels is strongly suppressed (black curve with full circles). Finally, the blue trace with open triangles shows the result of a calculation without spin–orbit coupling for a similar PA detuning, for which the PA levels exclusively decay towards the uppermost ground-state bound levels. The panel (a) of figure 4 shows the same calculation for the strongly resonant PA line of the $^{87}Rb_2$ molecule at a detuning of -4.87 cm^{-1} (red trace with full squares, $n = 475$ in our calculation), and for the weakly resonant line at -9.39 cm^{-1} (black trace with full circles). We observe a similar trend in both cases, with the peak in the population of ground-state vibrational levels shifted, and the amplitude of the FC factors changed.

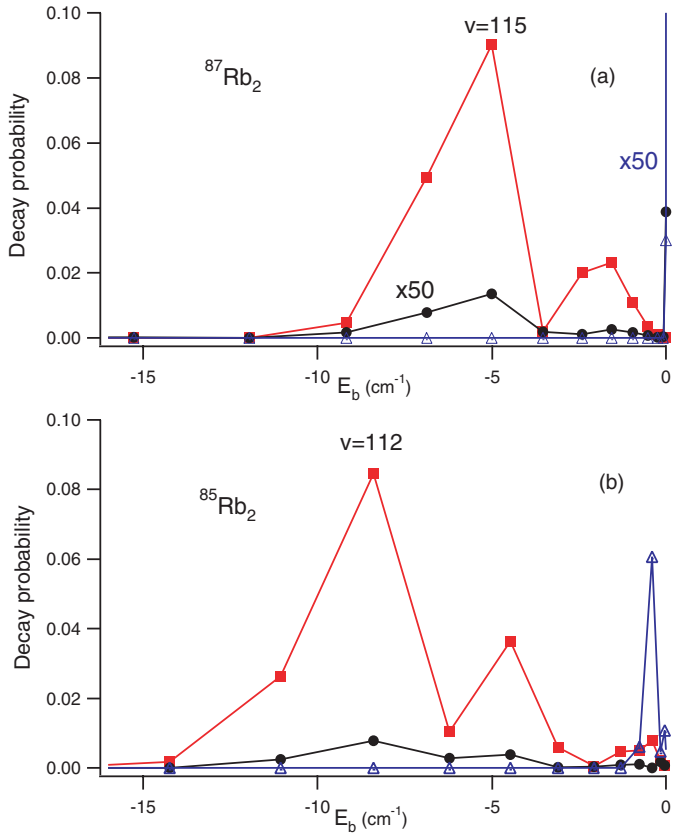

Figure 4. Decay probability for $^{87}Rb_2$ (a) and $^{85}Rb_2$ (b) molecule formation in the ground $X^1\Sigma_g^+$ state after PA through strongly coupled levels (red squares, $\delta_L = -4.87$ cm^{-1} for $^{87}Rb_2$ and $\delta_L = -54.26$ cm^{-1} for $^{85}Rb_2$) and through weakly coupled levels (black circles, $\delta_L = -9.39$ cm^{-1} for $^{87}Rb_2$ and $\delta_L = -49.00$ cm^{-1} for $^{85}Rb_2$). The vibrational levels of the ground singlet state with maximum decay probability are indicated for both isotopes. The blue triangles show the decay probability without spin–orbit coupling after PA at $\delta_L = -4.79$ cm^{-1} for $^{87}Rb_2$ and $\delta_L = -55.13$ cm^{-1} for $^{85}Rb_2$. The traces for $^{87}Rb_2$, with the exception of that at $\delta_L = -4.87$ cm^{-1}, are magnified by a factor 50 for clarity.

We modelled the cold molecule (CM) formation rate as already done in the previous publications [19] by computing the product of the free-bound FC factor for each PA level with the bound–bound FC factor for the decay step, summed over the levels of the ground state. We also computed the rotational constants B_v for each PA radial wavefunction. We assume that the ionization efficiency is similar for all created ground-state molecules, so that the computed CM rate can be directly compared to the experimental ionization signal, as shown in figure 5. Results for both isotopes are drawn on the same scale, for the purpose of comparing the interaction strength in both species. Looking first at $^{85}Rb_2$, we found a maximum of the CM rate for the PA detuning $\delta_L = -2.28$ cm^{-1} close to the observed maximum in the ion signal. While the recorded spectrum stops at -3.5 cm^{-1}, the width of the predicted signal is consistent with the experimental one. Two other lines associated with the presence of resonant coupling are also obtained around -9 cm^{-1} and -16 cm^{-1}, in agreement with the experimental observations reported by Bergeman *et al* [20].

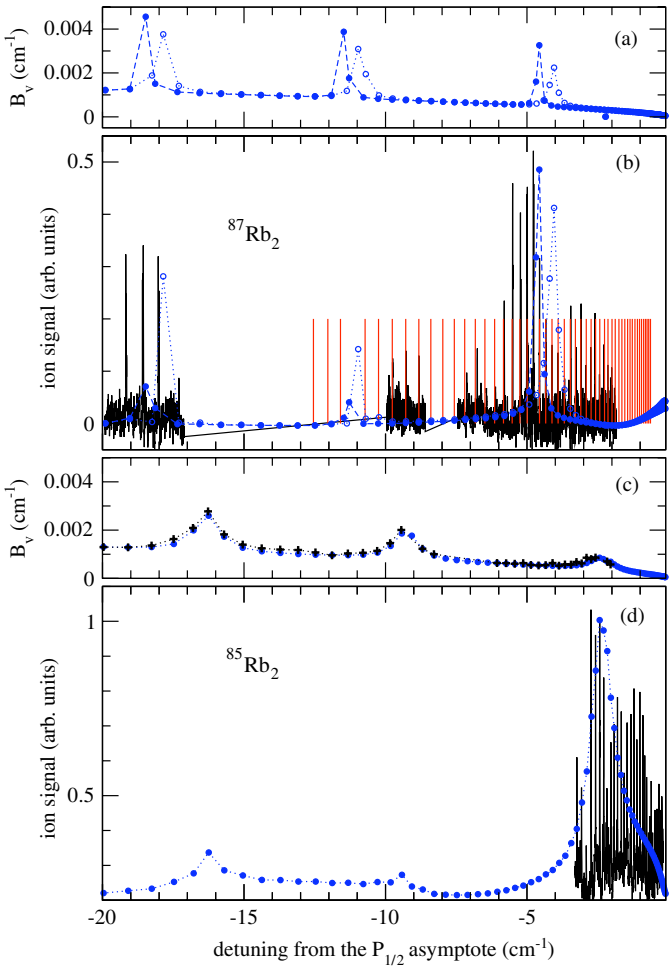

Figure 5. Comparison of the experimental ionization spectrum (black traces) in the investigated range of PA laser detunings δ_L with the modelled cold molecule formation rate (blue traces with circles, see text) for (b) $^{87}Rb_2$, and (d) $^{85}Rb_2$. For $^{87}Rb_2$, the position of lines measured in [22] are displayed as red vertical bars. Panels (a) and (c) show the corresponding calculated rotational constants. For $^{87}Rb_2$ (panels (a) and (b)), we performed two calculations: one by using the potentials and couplings of the $^{85}Rb_2$ molecule (open circles) and the other by adjusting them separately on the experimental signal (full circles). In panel (c), we displayed the experimental rotational constants (crosses) from [20] besides our calculations.

The presence of Rb_2^+ ions for low detunings outside the range of the main resonant feature of the spectrum (i.e. between -2 and 0 cm^{-1} in $^{85}Rb_2$, and between -2 and -4 cm^{-1} in $^{87}Rb_2$) is probably due to the ionization of molecules created in levels close to the ground-state dissociation limit. Such an ionization of high-lying vibrational levels is probably facilitated by the unusual flat potential well of the $2^1\Sigma_u^+$ state, which extends beyond $15a_0$ in the experimental ionization energy window (see figure 1). The ratio of the amount of such ions to the number of detected ions at the resonant feature is more important in $^{85}Rb_2$ than in $^{87}Rb_2$, which suggests that the resonant coupling is stronger in the latter case, so that the resonant feature is more prominent.

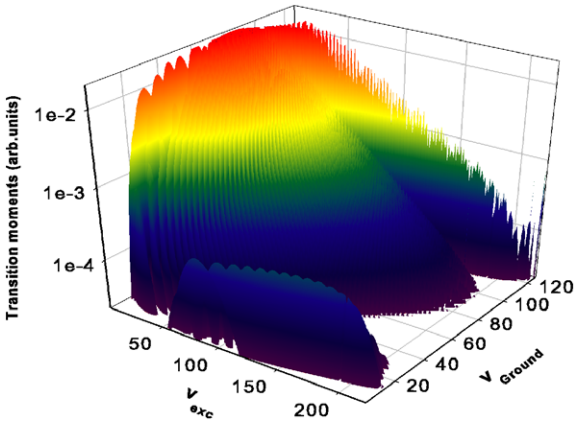

Figure 6. Transition moments for $^{85}Rb_2$ between vibrational levels of the ground singlet state to vibrational levels of the $2^1\Sigma_u^+$ state.

The present set of model potentials confirms this observation when the rotational constants are computed: they exhibit an oscillating pattern when levels below the $P_{1/2}$ asymptote are resonantly coupled to those converging towards the $P_{3/2}$ asymptote. Comparing panels (a) and (c) of figure 5, we find that the oscillations of B_v (which are also observed in [20]) are weaker in $^{85}Rb_2$ than in $^{87}Rb_2$, which is indeed an indication that wavefunctions are more strongly mixed in the latter case than in the former one.

The position of the main feature around $\delta_L = -5$ cm^{-1} in the $^{87}Rb_2$, agrees with the position of the step deduced in the quantum defect analysis of the trap loss spectrum of [22]. We modelled the $^{87}Rb_2$ spectrum using two hypotheses. We first employed the potentials and couplings from the $^{85}Rb_2$, and solved the coupled-state problem by simply changing the reduced mass. The computed position of the main features around the detunings $\delta_L = -5\,\text{cm}^{-1}$ and -18 cm^{-1} (open circles) is shifted towards lower detunings compared to the experimental ones. By slightly moving the repulsive wall of the $b^3\Pi_u$ state, we are able to obtain a better agreement for the energy position of the main features. This reflects that the resonant coupling cannot be described in both systems with a simple mass scaling, as it induces interferences between radial wavefunctions, involving their relative phases. It is important to note that the modification of the potential of the $b^3\Pi_u$ state does not change appreciably the decay probabilities shown in figure 4.

The molecules produced by resonant coupling in the ground singlet state are translationally and rotationally cold but, although part of them are quite deeply bound, they are created with a high internal vibrational energy. As demonstrated for RbCs in [42], an optical production of ultracold $v = 0$ molecules is possible by performing a further pump–dump transition through an excited state. Figure 1 suggests that the $2^1\Sigma_u^+(5s + 4d)$ state, used here as the first step of the REMPI detection process, should be a suitable choice. Indeed, we can expect that the ultracold ground-state molecules in high vibrational levels can be efficiently pumped into $2^1\Sigma_u^+(5s + 4d)$ levels, due to its flat well. At an excitation energy around 17 100 cm^{-1}, the reached levels (corresponding to $v \approx 50$, see figure 6) are predicted to have an internal turning point at $8a_0$, and would then directly decay, or could be pumped down, into the $v = 0$ level of the ground state. A similar mechanism was proposed for cesium [43].

4. Conclusions

In this paper, we observed for the first time the predicted isotopic effect in the formation of ultracold ground-state rubidium dimers. Despite the short range of photoassociation detuning explored in the experiment, we were able to identify in both rubidium isotopomers several photoassociation features induced by the resonant coupling of vibrational levels of the photoassociated states, enhancing the formation of ultracold molecules with a significant binding energy (up to 20 cm^{-1}). We modelled the ionization spectrum of the ultracold molecules, and deduced that the difference of rates between both isotopes cannot be entirely assigned to a simple mass scaling, but should involve the phase difference between the coupled wavefunctions of the photoassociated levels. Such resonantly coupled levels represent the first step of a promising path for the formation of ultracold rubidium dimers in their absolute ground level $v = 0$, that can be closed by pumping the produced dimers from a high to zero vibrational energy state by a pump–dump or a stimulated Raman adiabatic passage (STIRAP) scheme using another intermediate electronic state, like the $2^1\Sigma_u^+$ state.

Acknowledgments

This work is supported by RTN *Cold Molecules* (HPRN-CT-2002-00290). We gratefully acknowledge L Pruvost and E Luc-Koenig for helpful discussions.

Note added in proof. After proofreading, Dr C P Koch informed us about an independent study of the resonant coupling in $^{85}Rb_2$ by Pechkis *et al* [44].

References

[1] Dulieu O, Raoult M and Tiemann E 2006 *J. Phys. B: At. Mol. Opt. Phys.* **39** special edition
[2] DeMille D, Bay F, Bickman S, Kawall D, Krause D, Maxwell S E and Hunter L R 2000 *Phys. Rev.* A **61** 052507
[3] Hudson J J, Sauer B E, Tarbutt M R and Hinds E A 2002 *Phys. Rev. Lett.* **89** 023003
[4] Stwalley W C and Wang H 1999 *J. Mol. Spectrosc.* **195** 194
[5] DeMille D 2002 *Phys. Rev. Lett.* **88** 067901
[6] Bethlem H L, Berden G and Meijer G 1999 *Phys. Rev. Lett.* **83** 1558
[7] Jochim S, Bartenstein M, Altmeyer A, Hendl G, Riedl S, Chin C, Denschlag J H and Grimm R 2003 *Science* **302** 2101
[8] Greiner M, Regal C A and Jin D S 2003 *Nature* **426** 537
[9] Thorsheim H R, Weiner J and Julienne P S 1987 *Phys. Rev. Lett.* **58** 2420
[10] Masnou-Seeuws F and Pillet P 2001 *Adv. At. Mol. Opt. Phys.* **47** 53
[11] Mancini M W, Telles G D, Caires A R L, Bagnato V S and Marcassa L G 2004 *Phys. Rev. Lett.* **92** 133203
[12] Wang D, Qi J, Stone M F, Nikolayeva O, Wang H, Hattaway B, Gensemer S D, Gould P L, Eyler E E and Stwalley W C 2004 *Phys. Rev. Lett.* **93** 243005
[13] Kerman A J, Sage J M, Sainis S, Bergeman T and DeMille D 2004 *Phys. Rev. Lett.* **92** 033004
[14] Haimberger C, Kleinert J, Bhattacharya M and Bigelow N P 2004 *Phys. Rev.* A **70** 021402
[15] Kraft S D, Staanum P, Lange J, Vogel L, Wester R and Weidemüller M 2006 *J. Phys. B: At. Mol. Opt. Phys.* **39** S993
[16] Fioretti A, Comparat D, Crubellier A, Dulieu O, Masnou-Seeuws F and Pillet P 1998 *Phys. Rev. Lett.* **80** 4402
[17] Gabbanini C, Fioretti A, Lucchesini A, Gozzini S and Mazzoni M 2000 *Phys. Rev. Lett.* **84** 2814
[18] Fioretti A, Amiot C, Dion D M, Dulieu O, Mazzoni M, Smirne G and Gabbanini C 2001 *Eur. Phys. J.* D **15** 189
[19] Dion C M, Drag C, Dulieu O, Laburthe Tolra B, Masnou-Seeuws F and Pillet P 2001 *Phys. Rev. Lett.* **86** 2253
[20] Bergeman T, Qi J, Wang D, Huang Y, Pechkis H K, Eyler E E, Gould P L, Stwalley W C, Cline R A, Miller J D and Heinzen D J 2006 *J. Phys. B: At. Mol. Opt. Phys.* **39** S813
[21] Huang Y, Qi J, Pechkis H K, Wang D, Eyler E E, Gould P L and Stwalley W C 2006 *J. Phys. B: At. Mol. Opt. Phys.* **39** S857
[22] Jelassi H, Viaris de Lesegno B and Pruvost L 2006 *Phys. Rev.* A **74** 012510

[23] Koch C P, Kosloff R and Masnou-Seeuws F 2006 *Phys. Rev.* A **73** 043409
[24] Mur-Petit J, Luc-Koenig E and Masnou-Seeuws F 2006 *Preprint* phys/0612143v1
[25] Gerstenkorn S, Vergès J and Chevillard J 1982 *Atlas du spectre d'absorption de la molecule d'iode* (Orsay: Laboratoire Aimé Cotton)
[26] Pichler G, Milosevic S, Veza D and Vukicevic D 1983 *J. Phys. B: At. Mol. Phys.* **16** 4633
[27] Barwood G P, Gill P and Rowley W R A A 1991 *Appl. Phys.* B **53** 142
[28] Lozeille J, Fioretti A, Gabbanini C, Huang Y, Pechkis H K, Wang D, Gould P L, Eyler E E, Stwalley W C, Aymar M and Dulieu O 2006 *Eur. Phys. J.* D **39** 261
[29] Lisdat C, Dulieu O, Knöckel H and Tiemann E 2001 *Eur. Phys. J.* D **17** 319
[30] Amiot C, Dulieu O and Vergès J 1999 *Phys. Rev. Lett.* **83** 2316
[31] Cline R A, Miller J D and Heinzen D J 1994 *Phys. Rev. Lett.* **73** 632
[32] Kokoouline V, Dulieu O, Kosloff R and Masnou-Seeuws F 1999 *J. Chem. Phys.* **110** 9865
[33] Kokoouline V, Dulieu O, Kosloff R and Masnou-Seeuws F 2000 *Phys. Rev.* A **62** 032716
[34] Dulieu O, Julienne P and Weiner J 1994 *Phys. Rev.* A **49** 607
[35] Kokoouline V, Dulieu O and Masnou-Seeuws F 2000 *Phys. Rev.* A **62** 022504
[36] Kokoouline V, Vala J and Kosloff R 2001 *J. Chem. Phys.* **114** 3046
[37] Seto J Y, Le Roy R J, Vergès J and Amiot C 2000 *J. Chem. Phys.* **113** 3067
[38] van Kempen E G M, Kokkelmans S J J M F, Heinzen D J and Verhaar B J 2002 *Phys. Rev. Lett.* **88** 093201
[39] Edvardsson D, Lunell S and Marian C M 2003 *Mol. Phys.* **101** 2381
[40] Manaa M R, Ross A J, Martin F, Crozet P, Lyyra A M, Li L, Amiot C and Bergeman T 2002 *J. Chem. Phys.* **117** 11208
[41] Beuc R, Movre M, Horvatic V, Vadla C, Dulieu O and Aymar M 2007 *Phys. Rev.* A **75** 032512
[42] Sage J M, Sainis S, Bergeman T and DeMille D 2005 *Phys. Rev. Lett.* **94** 203001
[43] Pichler M, Stwalley W C, Beuc R and Pichler G 2004 *Phys. Rev.* A **69** 013403
[44] Pechkis H K, Wang D, Huang Y, Eyler E E, Gould P L, Stwalley W C and Koch C P 2007 *Phys. Rev.* A in press